12th International Symposium on Turbulence and Shear Flow Phenomena (TSFP12)
Osaka, Japan (Online), July 19-22, 2022

DISSIMILARITY BETWEEN THERMAL AND FLOW FIELDS IN TURBULENCE PIPE FLOW WITH CIRCUMFERENTIALLY-VARYING SURFACE HEAT FLUX

Yasuo Hattori
Sustainable System Research Laboratory
Central Research Inst. of Electric Power Industry
1646 Abiko, Abiko-shi, Chiba-ken, 270-1194, Japan
yhattori@criepi.denken.or.jp

Yuma Hasebe
Numerical Analysis Group
Denryoku Computing Center, Ltd.
3-5-1 Kanda-nishiki, Tokyo, 101-0054, Japan
hasebe@dcc.co.jp

Hitoshi Suto
Sustainable System Research Laboratory
Central Research Inst. of Electric Power Industry
1646 Abiko, Abiko-shi, Chiba-ken, 270-1194, Japan
suto@criepi.denken.or.jp

Keisuke Nakao
Sustainable System Research Laboratory
Central Research Inst. of Electric Power Industry
1646 Abiko, Abiko-shi, Chiba-ken, 270-1194, Japan
nakao@criepi.denken.or.jp

Shuji Ishihara
Numerical Analysis Group
Denryoku Computing Center, Ltd.
3-5-1 Kanda-nishiki, Tokyo, 101-0054, Japan
ishihara@dcc.co.jp

ABSTRACT

We performed well-resolved LESs for a turbulence pipe flow under a circumferentially-varying surface heat flux. After confirming the agreement of turbulence statistic with previous DNSs through discussion on dependencies numerical parameters, such as a domain size, grid resolutions, SGS models, we examined effects of the surface heat flux on turbulence characteristics of temperature fields in the boundary layer, especially paying attention to dissimilarities with velocity fields. The surface heat flux distributions increased temperature fluctuations and also activated intermittent entrainment motions with high temperature fluids near the heating start points. The entrainment motions weakened negative correlations between streamwise velocity with increasing in characteristic length of temperature fields. Such modulation in large-scale structures of temperature fields must be an origin of dissimilarities with velocity fields.

INTTRODUCTION

Turbulent pipe flows under non-homogeneous heat conditions along the azimuthal direction are still unknown, while turbulence characteristics of pipe flows under isothermal conditions, including without surface heating, have been widely investigated by using experiments and numerical simulations; previous studies have mainly focused on ideal thermal conditions, such as isothermal or uniform heat flux conditions. Indeed, as far as the authors know, there exists only one article dealing with a circumferentially-varying heat flux condition (Antoranz et al., 2015), whereas such a condition is one of the most simple configuration on non-homogeneous thermal conditions and also is of practical interest in engineering applications relating to solar radiation, e.g. heat removal design for solar power towers (Antoranz et al., 2015). The article mainly discussed on the reproductively of turbulence statistics with RANS models and suggested that corrections to the model with a constant turbulent Prandtl numbers are needed. This suggestion also implies the dissimilarity between thermal and flow fields, but the origin of the dissimilarity has not been discussed yet.

In the present study, to clarify the origin of the dissimilarity, we have carried out well-resolved LESs for a turbulence pipe flow with circumferentially-varying heat flux. The Reynolds numbers normalized with the pipe radius and the friction velocities were set to 180 and 360, corresponding to the previous DNSs (Antoranz et al., 2015). After confirming the agreement of turbulence statistic with previous DNSs through discussion on dependencies numerical parameters, such as grid resolutions, SGS models, we investigated changes in turbulence characteristics of temperature fields in the boundary layer due to surface heat flux distributions and discussed differences with velocity fields. Reynolds number dependencies also examined by using comparison among two Reynolds number conditions.

NUMERICAL SET-UP

The object we considered here was a turbulence flow, which was a pressure-driven incompressible flow of a fluid with constant properties. The fluid temperature was simply treated as a passive scaler: the buoyancy was not considered. The thermal condition imposed at the wall was a circumferentially-varying heat flux given by a sine function ($q_w = \pi < q_w > \sin\theta$ for $0 < \theta < \pi$, and $q_w = 0$ for $-\pi < \theta < 0$; where $< q_w >$ and θ are the net heat flux at the wall and the azimuthal direction, respectively), which also mimics heat flux conditions of a pipe surface due to the sun radiation. The added heat leads to a net increase of the temperature along the axial direction, and thus we set a heat balance with the axial gradient of the bulk temperature. Two Re number and Pr number conditions were considered. The values of Re numbers normalized with the pipe radius and the friction velocities were set to 180 and

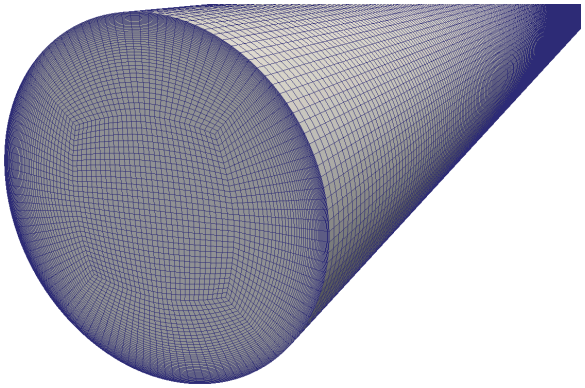

Figure 1. Grid arrangement.

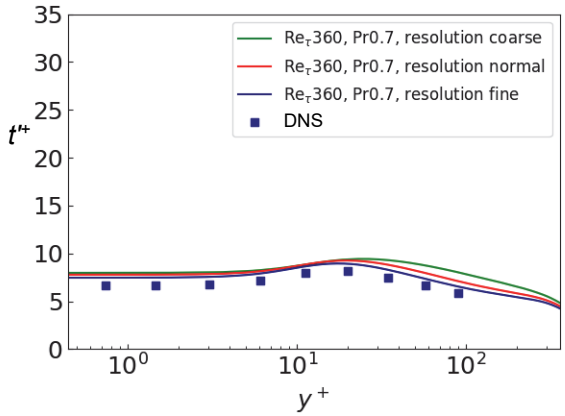

Figure 2. Profiles of r.m.s. values of temperature fluctuations in boundary layer at $\theta = \pi/2$ for Re_τ=360, Pr =0.7, predicted by various grid resolutions. The DNS data by Antoranz et al. (2015) are also plotted by squares.

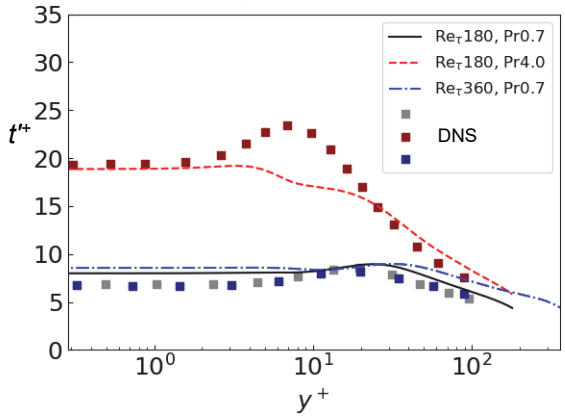

Figure 3. Profiles of r.m.s. values of temperature fluctuations in boundary layer at $\theta = \pi/2$ for Re_τ=180 and 360, Pr =0.7 and 4.0, predicted by Smagrinsky model. The DNS data by Antoranz et al. (2015) are also plotted by squares.

360 for two Pr number conditions, Pr = 0.7 and 4, corresponding to previous DNSs (Antoranz et al., 2015). However, this paper will mainly discuss the results for Pr = 0.7.

The LESs were carried out with an open source CFD code, OpenFOAM, which has been widely used all over the world for numerical turbulence simulating. The present simulation was based on a LES version with PIMPLEfoam of OpenFOAM, in which the option of RANS scheme was turn off. An anisotropy-resolving subgrid-scale model proposed by Abe (2013), which improves the predictive performance particularly for coarse grid resolution in the near-wall region, was adopted to represent the subgrid-scale diffusion. The Pr_{SGS} was set at 0.85. The differencing schemes for a limited-linear scheme for advection terms and a back Euler scheme for time integration were chosen.

The grid arrangement used in the present study is shown in Fig. 1, which ensured the alignment of numerical grids with flow patterns, e.g., the grid spacing changed with the distances from the pipe surface. The minimum grid level in the normal direction with the wall unit was set to 0.57 and 1.1 for Re_τ = 180 and 360, respectively, corresponding to previous DNS (Antoranz et al., 2015). The computational domain had a long of 100R, where R is the radius of the pipe. The domain size is quite large compared with previous studies; this is because that recent studies (e.g. Guala et al., 2006; Monty et al. 2007; Lee et al., 2019) have suggested that the coherence structure, which has a large characteristics length in the streamwise direction, play in an important role in turbulence transport phenomena of boundary layer flows.

The statistics were estimated by the Reynolds decomposition for the time-series during 150 – 300, normalized with the wall units when there exists no increasing or decreasing tendencies of the bulk parameters and fluctuation components of velocities and temperature against time.

Firstly, we checked the dependencies of numerical parameters, such as the SGS model, grid resolutions, domain size, on profiles of turbulence statistics. Figures 2 and 3 show examples of r.m.s. values of temperature fluctuations, t', predicted by various grid resolutions and SGS models. The DNSs data (Antoranz et al. 2015) are also plotted in the figures. The profiles in the boundary layer at $\theta = \pi/2$, where the r.m.s. value takes maximum value, are presented. The profiles are normalized with the inner parameters, i.e., the friction velocity, u_τ, the kinetic viscosity, and the friction temperature, $t_\tau = \langle q_w \rangle / \rho C p u_\tau$, where ρ, Cp are density and constant pressure specific heat of the working fluid, respectively. The normal grid resolution used in the present LESs gives good agreement with DNSs, while LESs and DNSs are naturally in better agreement with finer grid resolutions. Also, the profiles predicted with Abe model agree well with those by DNSs, whereas the profiles predicted by Smagrinsky model apparently differ from those by DNSs, regardless to Re and Pr numbers. Notice that, the profiles of r.m.s. values of temperature fluctuations clearly showed the domain-size dependencies, i.e., the r.m.s. values near the wall with the domain size of 5R are significantly larger than those with the domain size of 100R; these overestimates of r.m.s values with the domain size of 5R occur regardless to conditions, Re and Pr, which indicates the necessity of large domain size. Moreover, we examined the profiles of statistics in velocity fields under the homogeneous heat conditions and confirmed the profiles predicted by Abe model with normal grid resolution, including the near-wall region, agree well with those obtained DNSs reported by previous studies (Fukagata and Kasagi, 2002; Piller, 2005), including the Re number effects which give increases in r.m.s. values and extensions of the logarithmic layer to outer regions.

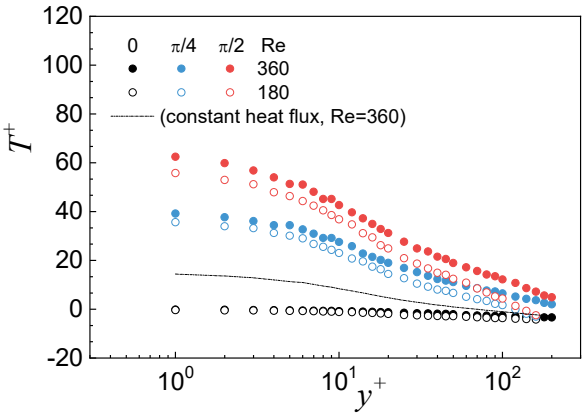

Figure 4. Profiles of time-averaged values of temperature in boundary layer at $\theta = 0$, $\pi/4$, $\pi/2$.

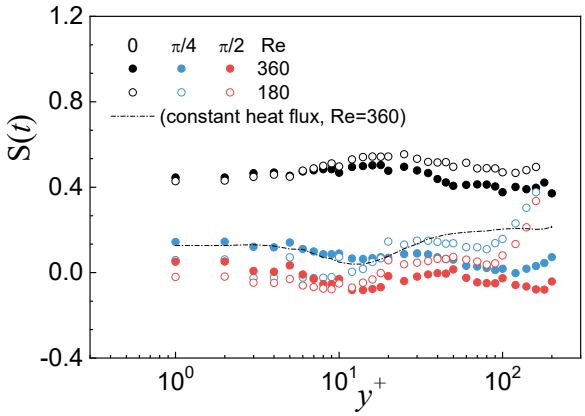

Figure 6. Profiles of skewness factors of temperature in boundary layer at $\theta = 0$, $\pi/4$, $\pi/2$.

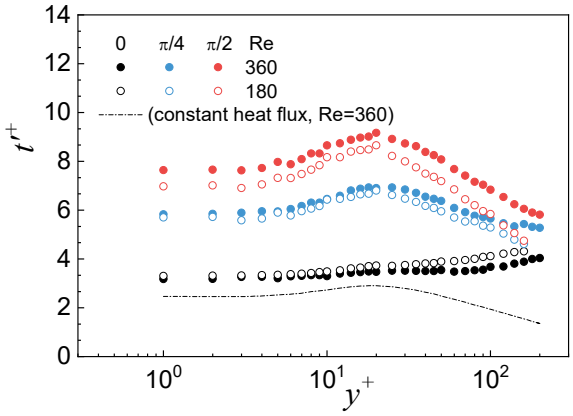

Figure 5. Profiles of r.m.s. values of temperature in boundary layer at $\theta = 0$, $\pi/4$, $\pi/2$.

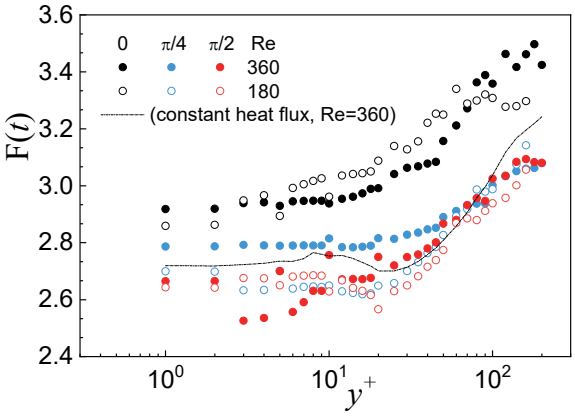

Figure 7. Profiles of flatness factors of temperature in boundary layer at $\theta = 0$, $\pi/4$, $\pi/2$.

RESULTS AND DISCUSSION

Profiles of time-averaged values of temperature, T, in the boundary layer at $\theta = 0$, $\pi/4$, $\pi/2$ are presented in Fig. 4. The results under constant heat flux condition, the net heat flux of which consistent with the present value, are also plotted in the figure. The temperature in the boundary layer essentially increases with θ, which is due to the circumferentially-varying heat flux given by a sine function. The Reynolds number dependencies seem to be small, while the temperature in the outer layer of boundary layer slightly decreases with Reynolds numbers.

Figure 5 shows the profiles of r.m.s. values of temperature, t', in the boundary layer at $\theta = 0$, $\pi/4$, $\pi/2$ with that for constant heat flux condition. The r.m.s. values drastically increase with circumferentially-varying heat flux at the pipe surface. The r.m.s values in the boundary layer are apparently large compared with that for constant heat flux conditions, even at $\theta = 0$, where the time averaged temperature is much low. The maximum r.m.s. values in the boundary layer appear at $y^+ \cong 30$, except at $\theta = 0$. Also, the r.m.s values, regardless to azimuthal direction, naturally become constant approaching the center of the pipe. The Reynolds number dependencies seem to be small, while the r.m.s values in the outer layer of boundary layer slightly decreases with Reynolds numbers, except at $\theta = 0$.

The profiles of higher-order moments, skewness and flatness factors, S(t) and F(t), in the boundary layer are presented in Figs. 6 and 7. The positive value of skew factor with large flatness factor appear at $\theta = 0$, indicating the existence of intermittent entrainment motions with high temperature fluids. Such entrainment motions become more active in the outer layer for $Re_\tau = 180$. Here, I must stress that these factors give no evidence for generation of coherence structures in the near-wall region of thermal fields; the flatness factors gradually increase with y^+, whereas the flatness factors of streamwise velocities drastically increases in the near-wall region.

Figure 8 shows the profiles of cross-correlation between streamwise velocity and temperature in the boundary layer. They are negatively correlated in the whole region. Negative correlation in the boundary layer apparently weaken at $\theta = 0$ and also near the center of the pipe where the intermittent fluid motions become active. The Reynolds effects only appear near the center of the pipe, which rapidly decrease negative correlations between streamwise velocity and temperature.

Figure 9 depicts a snapshot of streamwise velocity and temperature in a cross section and a longitudinal section in the pipe. The flow and thermal fields in the cross section for $\theta > 0$, show the high-speed regions with low temperature flows even near the wall with the organized patterns against the azimuthal direction, corresponding to helically inclined structures (Ahn and Sung, 2017). Such structures in the thermal field gradually diminish for $\theta < 0$, yielding the asymmetric patterns in the

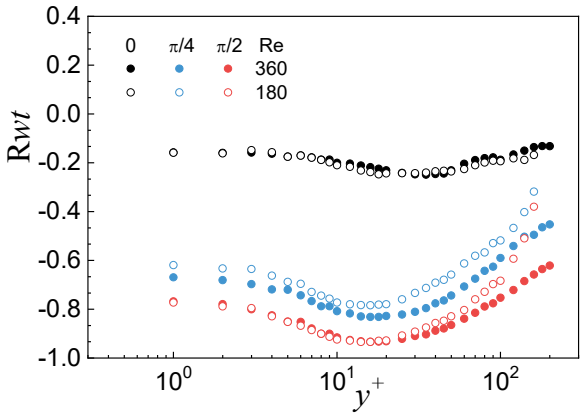

Figure 8. Profiles of cross-correlation between streamwise velocity and temperature in boundary layer at $\theta = 0$, $\pi/4$, $\pi/2$.

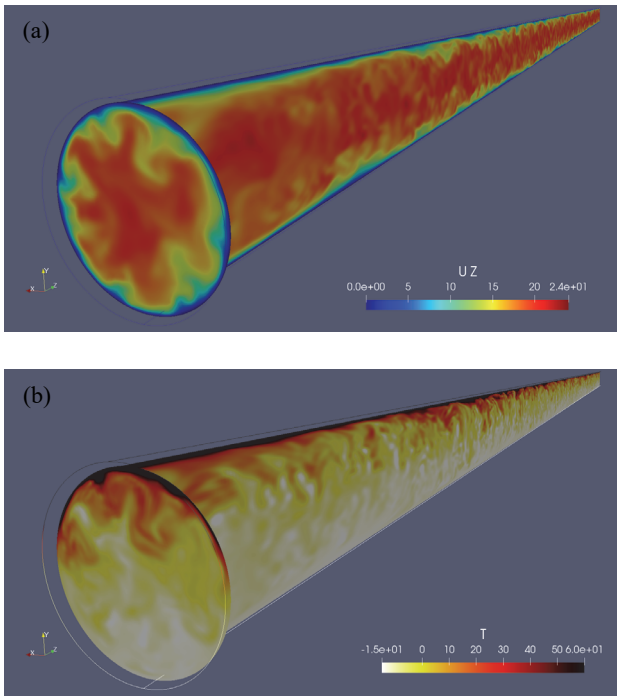

Figure 9. Snapshot of contour of streamwise velocity, (a), and temperature (b), normalizing with the inner parameters for $Re_\tau = 360$.

cross and longitudinal sections.

Snapshots of fluctuations of temperature and streamwise velocity at $y^+ = 3$, 30 and 150 by a view with transformation from the true to the Cartesian (s-z) coordinates, where $s = r\theta$, according to previous studies (Monty et al., 2007; Hellström and Smiths, 2017) for $Re_\tau = 360$ are presented in Figs. 10 and 11. Normalization was done by the inner parameters. Low- and high-speed regions elongated in the streamwise direction with meandering in the spanwise direction are generated in the flow fields, regardless to the azimuthal position. The length of low- and high-speed regions in the streamwise direction sometimes exceed 25R, while such structures seem to different intensities and characteristic lengths against the distance from the pipe surface. Contrary to the flow fields, the thermal fields significantly depend on the azimuthal position, while the region

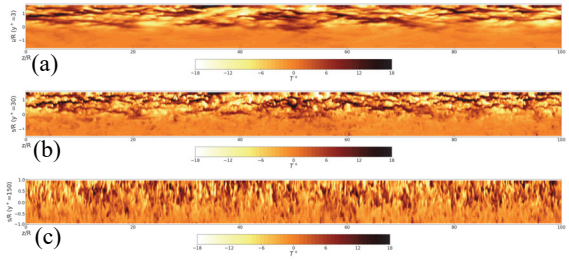

Figure 10. Snapshot of contour of temperature fluctuations at $y^+ = 3$, (a), 30, (b), and 150, (c), normalizing with the inner parameters for $Re_\tau = 360$.

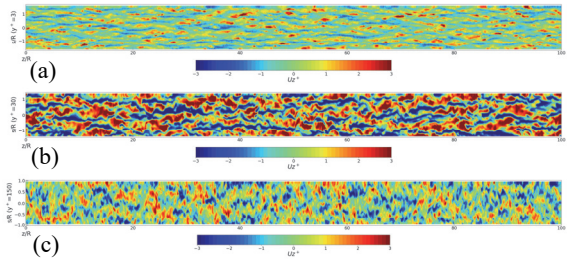

Figure 11. Snapshot of contour of fluctuations of streamwise velocity at $y^+ = 3$, (a), 30, (b), and 150, (c), normalizing with the inner parameters for $Re_\tau = 360$.

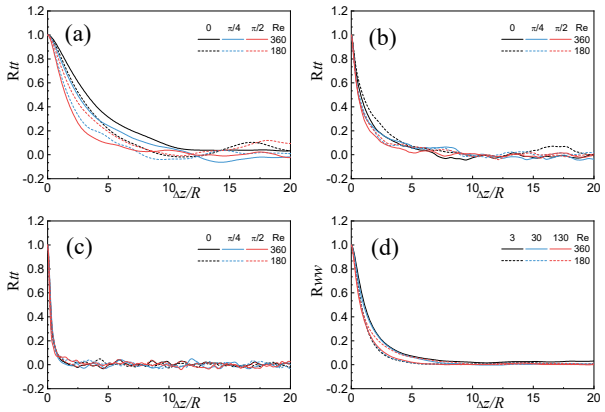

Figure 12. Two point correlation in streamwise direction of temperature at $y+ = 3$, (a), 30, (b), 150, (c), and streamwise velocity, (d).

of $s/R > 0$, where the heat flux at the surface is positive, generates low- and high-temperature patterns elongated in the streamwise direction.

Figure 12 shows two-point correlations of streamwise velocities and temperatures fluctuations in the streamwise direction at $y^+ = 3$, 30, 150. These correlations clearly show the differences of characteristics lengths in the streamwise direction between the flow and the thermal fields. The characteristics length of the flow fields gradually increases with distances from the pipe surface. On the other hands, the characteristics length of the thermal fields strongly depends on azimuthal positions as well as distances from the pipe surface, and the longest characteristic length appears at $\theta = 0$ of near-wall region ($y^+ = 3$). This length significantly large compared with the characteristics length of streamwise velocities.

These results indicate that the circumferentially-varying heat flux at the pipe surface increased temperature fluctuations and also activated intermittent entrainment motions with high temperature fluids due to heterogeneous surface heat flux along the azimuthal directions. The entrainment motions weakened negative correlations between streamwise velocity with increasing in characteristic length of temperature fields. Such modulation in large-scale structures of temperature fields must be an origin of dissimilarities with velocity fields. Such large-scale structures might be related to the helically included structures in the pipe (Ahn and Sung, 2017). On the other hands, the relationship with very large-scale motions (VLSMs), which are energetic, typically containing half of the turbulence kinetic energy of the streamwise component, and with the characteristic length of $25R$ in the streamwise direction of logarithmic layer (Guala et al., 2006; Monty et al., 2007; Hellström and Smits, 2017; Lee et al., 2019) should be carefully examined with helps of additional LESs for high Reynolds number conditions. The Reynolds number of the present LESs are apparently small compared with that for experiments to examine VLSMs. Monty et al. (2007) experimentally investigated the features of VLSMs of turbulence pipe flows with the range of Re_τ from 615 to 4355 and confirmed the existence of VLSMs regardless to Reynolds number. We have a plan to carry out the LESs at $\mathrm{Re}_\tau = 615$.

CONCLUSIONS

We have carried out well-resolved LESs for a turbulence pipe flow with circumferentially-varying heat flux, especially paying attention to the dissimilarity between temperature and velocity fields; the previous DNSs (Antoranz et al., 2015) suggested that corrections to the model with a constant turbulent Prandtl numbers are needed, implying the dissimilarity. The Reynolds numbers normalized with the pipe radius and the friction velocities were set to 180 and 360, corresponding to the previous DNSs. After confirming the agreement of turbulence statistic with previous DNSs and also dependencies numerical parameters, such as grid resolutions, SGS models, we investigated changes in turbulence characteristics of temperature fields in the boundary layer due to surface heat flux distributions and discussed differences from velocity fields. The surface heat flux distributions, which increase temperature fluctuations in the boundary layer, activated intermittent entrainment motions and weakened negative correlations between streamwise velocity with increasing in characteristic length of temperature fields. Such modulation in large-scale structures of temperature fields must be an origin of dissimilarities with velocity fields.

REFERENCES

Abe, K., 2013, “An improved anisotoropy-resolving subgrid-scale model with the aid of a scale-similarity modelling concept,” *Int J Heat Fluid Flow*, Vol. 29, pp. 42-52.

Ahn, J., and Sung, H.J., 2017, “Relationship between streamwise and azimuthal length scales in a turbulent pipe flow,” *Phys Fluids*, Vol. 29, 105112.

Antoranz, A., Gonzalo, A., Flores, O., and Garcia-Villalba, M., 2015, “Numerical simulation of heat transfer in a pipe with non-homogeneous thermal boundary conditions,” *Int J Heat Fluid Flow*, Vol. 55, pp. 45-51.

Fukagata, K., and Kasagi, N., 2002, “Highly energy-conservative finite difference method for the cylindrical coordinate system,” *J Comp Phys*, Vol.181, pp. 478-498.

Guala, M., Hommema, S.E., and Adrian, R.J. 2006, “Large-scale and very-large-scale motions in turbulent pipe flow,” *J Fluid Mech*, Vol.554, pp. 521-542.

Hellström, L.H.O., and Smits, A.J., 2017, “Structure identification in pipe flow using proper orthogonal decomposition,”, *Phil Trans R Soc A*, Vol. 375, 20160086.

Lee, J.H., Sung, H.J., and Adrian, R.J. 2019, “Space-time formation of very-large-scale motions in turbulent pipe flow,” *J Fluid Mech*, Vol.881, pp. 1010-1047.

Monty, J.P., Stewart, J.A., Williams, R.C., and Chong, M.S., 2007, “Large-scale features in turbulent pipe and channel flows,” *J Fluids Mech*, Vol. 589, pp. 147-156.

Piller, M., 2005, “Direct numerical simulation of turbulent forced convection in a pipe,” *Int J Numerical Methods in Fluids*, Vol. 49, pp. 583-602.